

THE FATIGUE OF HIGHLY FORMED BODIES

JAROMIR KASPAR¹, PETR BERNARDIN¹, VACLAVA LASOVA¹

University of West Bohemia, Faculty of Mechanical Engineering,
Department of Machine Design

DOI: 10.17973/MMSJ.2023_10_2023039

jkaspar@fst.zcu.cz

Fatigue of cold formed parts is an important consideration especially in the automotive industry. Methods exist for predicting the fatigue of parts where the plastic deformation during forming is less than the uniform elongation. Nevertheless, many stamped parts include areas where forming strain exceeds uniform elongation. These areas are also very important in terms of high cyclic fatigue. Fatigue tests were carried out on these highly formed bodies. The results are presented in this paper. Also, a simple method is proposed for avoiding some common mistakes in fatigue evaluation.

KEYWORDS

High cyclic fatigue, forming, Forming limit diagram, plastic strain, erfh5

1 INTRODUCTION

Research of fatigue in cold formed parts is important for many reasons. Cold forming is widely undertaken on forming machines [Chval 2016, Raz 2020], primarily in the automotive industry. This business sector has high demands in terms of reliability. There are also high demands on the development process. New cars and components have to be developed in a short time and the price of the development process has to be reduced too. This leads to a preference of simulation methods [Chval 2020] over physical testing which is expensive and time consuming. The lifetime of components is influenced by many factors such as stamping, welding or surface coating. Methods which enable the consideration of the effects of plastic strain originating during forming exist and are available in commercial fatigue software. Examples of these methods include the Material Law of Steel Sheet (MLSS) and the Method of Variable Slopes (MVS) implemented in FEMFAT software. These methods assume that effective plastic strain originating during forming does not exceed uniform elongation. Other researchers have also made similar assumptions [Le 2009]. Fatigue results for specimens where pre-strain is higher than uniform elongation are not available.

From our measurements it is clear that if effective plastic strain originating during forming exceeds uniform elongation then results based on MVS or MLSS are no longer valid. These methods should be adjusted to situations when effective plastic strain is high. Unfortunately, if these methods are implemented in proprietary software, it is not possible to modify them. This paper proposes a simple method to evaluate the fatigue of the stamped part which includes areas of both low and high effective strain. Direct modification of MVS or MLSS is not needed, so proprietary fatigue software can be used. The method proposed here is valuable for practical use because it prevents erroneous results.

2 PROBLEM DESCRIPTION

There are two areas which need to be investigated. The first area is forming. It is necessary to check if the formed part can be produced without defects. It is also useful to evaluate effective plastic strain, wall thinning or residual stress which can be used

in further evaluation of fatigue. The second area is evaluation of life-time where forming effects are taken into account. Calculation of a stamped part's fatigue which considers forming effects can be seen in [Meng 2013] and [Jakubec 2022] in detail.

2.1 Forming

It is common practice to use a Forming Limit Diagram (FLD) to evaluate formability. The FLD where levels of effective plastic strain are visualized was originally published in [Massendorf 2000]. A similar FLD is shown in Figure 1. This diagram shows that it is possible to produce a stamped part where effective plastic strain exceeds uniform elongation.

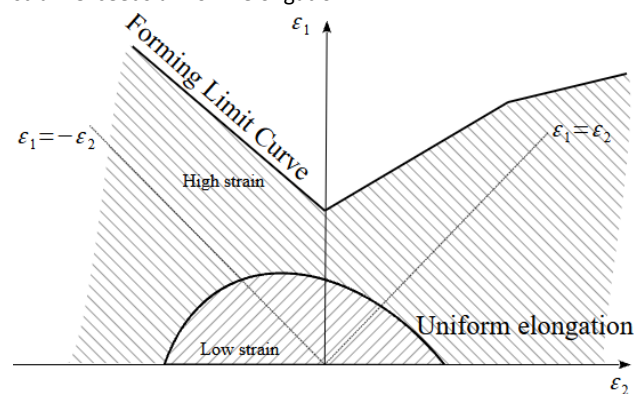


Figure 1. Forming Limit Diagram (FLD)

It should be noted that the FLD was drawn for flat pre-strained specimens. A flat specimen has the same plastic strain on the top surface, in the middle surface and on the bottom surface. This is not valid for pre-strained parts with non-zero curvature. Creating the same diagram for such a part is difficult. The FLD is valid for the middle surface [Abspoel 2013], but effective plastic strain needed for fatigue evaluation should be evaluated on the part's surface. High cyclic fatigue cracks are nucleated on the surface.

2.2 Fatigue

MVS and MLSS methods prescribe a strain life curve based on pre-strain level. The pre-strain level is expressed via effective plastic strain φ_v , formula (1) which is based on [FEMFAT 2022]. Symbols ε_1 , ε_2 , ε_3 represent principal plastic strains calculated via Finite Element Method (FEM).

$$\varphi_v = \sqrt{\frac{2}{3} \{ [\ln(\varepsilon_1 + 1)]^2 + [\ln(\varepsilon_2 + 1)]^2 + [\ln(\varepsilon_3 + 1)]^2 \}} \quad (1)$$

The author of the MLSS method published it in the form of equation (2) in his work [Massendorf 2000].

$$\varepsilon_a = \frac{(10370 + 13036\varphi_v)}{EA_g} (2N)^{-0.065} + (1.5262 - 1.1878\varphi_v)\rho(2N)^{-0.518} \quad (2)$$

E represents Young's modulus, ε_a is strain amplitude, A_g is uniform elongation entered in percentage, N is number of cycles and ρ is exponent of power law (3) which is an approximation of the cyclic stabilized stress-strain curve. Symbol σ represents true stress, ε is true strain and κ is constant.

$$\sigma = \kappa \varepsilon^\rho \quad (3)$$

The MVS is taken from [Hatscher 2004] in the form of equation (4). Constants γ , ω , α , β , $N_{0.2}$, E can also be found in [Hatscher 2004]. For material S420MC $\gamma=0.7$, $\omega=1.6$, $\alpha=0.0041$, $\beta=0.69$, $N_{0.2}=7500$ and $E=206000$ MPa. Ultimate strength R_m is 480 MPa.

$$\begin{aligned} \varepsilon_a &= \frac{\gamma R_m (1 + \varphi_v)}{E} \left(\frac{N}{N_{0.2}} \right)^a + 0.002 \left(\frac{N}{N_{0.2}} \right)^b \\ a &= \frac{-1}{\log(2N_{0.2})} \log \left[\frac{\omega}{\gamma(1 + \varphi_v)} \right] \\ b &= \frac{\log \left[\frac{0.002E}{\gamma R_m (1 + \varphi_v)} \right]}{\log[\alpha \gamma R_m (1 + \varphi_v) - \beta]} + \\ &\quad - \frac{1}{\log(2N_{0.2})} \log \left[\frac{\omega}{\gamma(1 + \varphi_v)} \right] \end{aligned} \quad (4)$$

The strain life curve as a function of φ_v is shown in Figure 2, where relationships (2) and (4) are visualized as ε_a - N - φ_v surfaces. The authors of the MVS and MLSS methods point out in their publications [Massendorf 2000], [Hatscher 2004] that results are valid only if effective plastic strain does not exceed uniform elongation A_g . Implementation of both methods in FEMFAT does not have a ceiling and the fatigue curve is changed for any φ_v as indicated by the arrow in Figure 2. Increase of lifetime could continue even if effective plastic strain significantly exceeds uniform elongation. This could lead to life-time overestimation if the results are not checked carefully. In FEMFAT ε_a is replaced by stress amplitude σ_a , i.e. S - N curve is used. The replacement is done with the use of cyclic stabilized stress-strain curve.

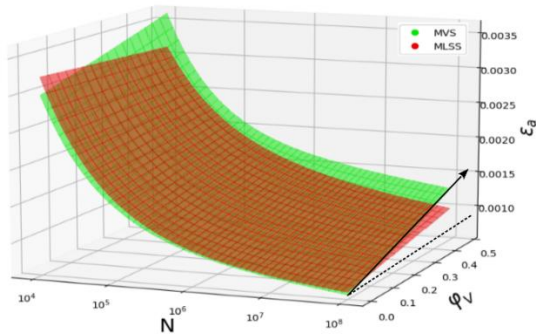


Figure 2. Strain life curve as a function of effective plastic strain φ_v (ε_a - N - φ_v surface)

3 EXPERIMENTS AND CALCULATIONS

Fatigue calculation of a stamped part has several steps. It is necessary to calculate the forming effects, primarily the effective plastic strain. Also, operational stress emerging during cyclic loading has to be analysed. Both calculations are done using FEM. If the mesh used in the forming task differs from the mesh used in the operational stress analysis, then the results from the first task have to be mapped onto the mesh of the second task. All the results are then transferred into the fatigue software, where fatigue is evaluated. The local approach is used, i.e. the S - N curve is adjusted for each mesh node depending on the conditions in it. One of the local influence factors is effective plastic strain.

The specimens which we used for the tests and which are described below always have two planes of symmetry. The symmetry can be used to simplify the calculation model. Therefore, models used for forming simulations were cut according to symmetry planes – this is referred to as the “reduced model” in the following sections. Appropriate boundary conditions were applied to these cuts.

Forming simulations were done in accordance with [Jakubec 2022]. A multilinear stress-strain curve with isotropic hardening was used. Parts are made from rolled metal sheet which has orthotropic behaviour, therefore, Hill’s 1948 yield criterion [Hill 1948] was used. M. Jakubec in his work [Jakubec 2022] derived the necessary parameters for S420MC. He prepared the material specimens in the rolling direction, perpendicular to the rolling direction and 45° to the rolling direction. Then he performed tensile tests and test simulations. An optimization procedure was used to derive the material parameters. Tensile tests were supplemented by compression tests. Jakubec’s material model of S420MC was used in all of our forming simulations.

The results from the forming simulations were extended to full-size models via script. Models, without any reduction, were used for operational stress calculation and for fatigue evaluation. FEMFAT fatigue software uses stress gradient [FEMFAT 2022] for fatigue evaluation. The stress gradient influence was active in our calculations. This is because the curvature of some of the specimens is high. Significant stress peaks occurred in areas of high curvature. The stress gradient in the nodes is calculated from the surrounding elements. If some elements were missing due to the model’s reduction, then stress gradient and fatigue results around the cuts would be incorrect.

The Scaled Normal Stress (SNS) method [Wächter 2022] was used to calculate the mean stress and stress amplitude which are important for fatigue evaluation. Normal stresses $\sigma_{ni,j}$ are calculated in this method for each normal direction given by vector $\{n_i\}$ according to formula (5). Stress matrix $[\sigma_j]$ is related to the j^{th} load-step. Normal stresses $\sigma_{ni,j}$ can be used for stress amplitude calculation and mean stress calculation in each direction $\{n_i\}$. The direction with the highest damaging effect is chosen.

$$\sigma_{ni,j} = \left(1 + \left(1 - \frac{\sigma_e}{\tau_e} \right) \right) w \{n_i\}^T [\sigma_j] \{n_i\} \quad (5)$$

Formula (5) also contains shear strength τ_e and normal strength σ_e . The ratio of σ_e and τ_e can be understood as a measure of ductility as [Wächter 2022] explains. Symbol w is the ratio of principal stresses given by formula (6).

$$w = \begin{cases} \frac{\sigma_3}{\sigma_1}, & \text{if } |\sigma_1| \geq |\sigma_3| \\ \frac{\sigma_1}{\sigma_3}, & \text{if } |\sigma_3| > |\sigma_1| \end{cases} \quad (6)$$

Normal directions $\{n_i\}$ are chosen with constant step. Figure 3 shows normal vectors with step $\delta=30^\circ$ because of clarity. Step $\delta=10^\circ$ was used in our calculations.

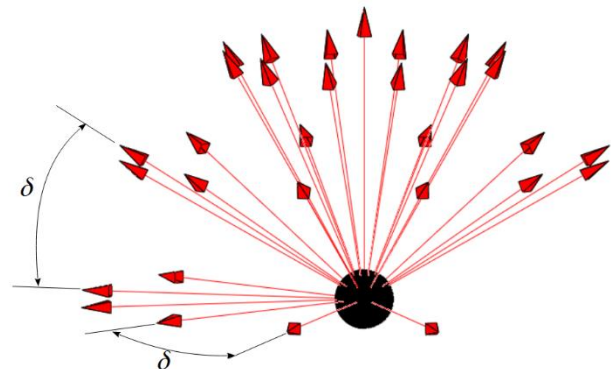


Figure 3. Normal directions

Four specimen types were prepared to test this calculation procedure and check the validity of MLSS and MVS especially for high strains.

3.1 Specimen A

Type A specimens had an effective plastic strain in the critical spot of about 8% which is less than the uniform elongation of the material S420MC. The mechanical properties and chemical composition of this material can be seen in [Martinez 2019], and fatigue properties are given in [Klemenc 2015]. The uniform elongation of this material is 13% according to our measurements. The specimens were exposed to symmetric compression-tension load cycles with three different amplitudes. Specimens with Zn-Ni surface coating and specimens without surface treatment were tested. The dimensions of the specimens are shown in Figure 4. The arrows marked *F* show the direction of the loading force. Constant bending stress occurred in the specimen in the testing machine, because the left flat part of the specimen is not parallel with the right flat part of the specimen. This is a consequence of the spring-back effect. Mean stress influence was considered in all calculations using the High diagram.

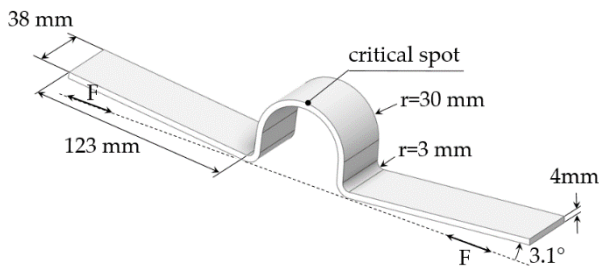


Figure 4. Dimensions of specimen A

Figure 5 shows a comparison of the experimental results with the calculated results. Three calculation methods were used. The first was MVS, the second MLSS and the third calculation method did not consider the effect of plastic strain at all. Fatigue was evaluated for two different surface roughnesses. The surface roughness $R_z=8 \mu\text{m}$ is related to parts without surface coating. The surface roughness $R_z=13 \mu\text{m}$ is related to parts with surface coating. Both roughness values are based on measurements. Calculations considered roughness according to [FKM 2003]. This means that the surface roughness factor K_R was calculated according to formula (7).

$$K_R = 1 - a_R \log(R_z) \log\left(\frac{2R_m}{R_{m,N,min}}\right) \quad (7)$$

The constant a_R for steel is equal to 0.22 and $R_{m,N,min}$ is 400 MPa. The *S-N* curve was then multiplied by factor K_R in order to reflect the influence of roughness.

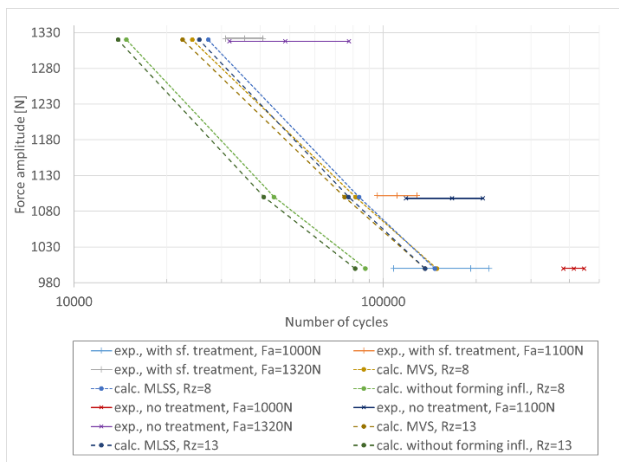


Figure 5. Specimen A – Comparison of experiments (exp.) and calculations (calc.)

Figure 5 shows that MLSS and MVS provided slightly conservative results. If the effect of plastic strain is not taken into account then the results are highly conservative.

[Massendorf 2000] and [Hatscher 2004] claim that residual stress relaxation is nearly complete if stress amplitude reaches yield strength. Its minimum value is 420 MPa. All calculations assumed a complete relaxation of residual stress, regardless of stress amplitude. This is because consideration of stress relaxation in the calculation model is a complex task, and there is no clear procedure for how to perform it.

Calculated mean stresses and stress amplitudes in critical spots for each loading level are shown in Table 1. A linear material model was used for operational stress analysis. Then the mean stress rearrangement via the Neuber hyperbola [FEMFAT 2022] was used.

Force amplitude [N]	Stress amplitude [MPa]	Mean stress [MPa]
1320	510	40
1100	422	49
1000	383	50

Table 1. Mean stress and stress amplitude in critical spot of specimen A

Specimen A with a fatigue fracture is shown in Figure 6. This specimen was tested with a force amplitude of 1320 N. The specimen's surface was not protected with a coating.



Figure 6. Specimen A after testing

Figure 7 shows the calculated number of cycles until crack initiation. Force amplitude was 1320 N, surface roughness was $R_z=8 \mu\text{m}$ and MLSS was used in this case.

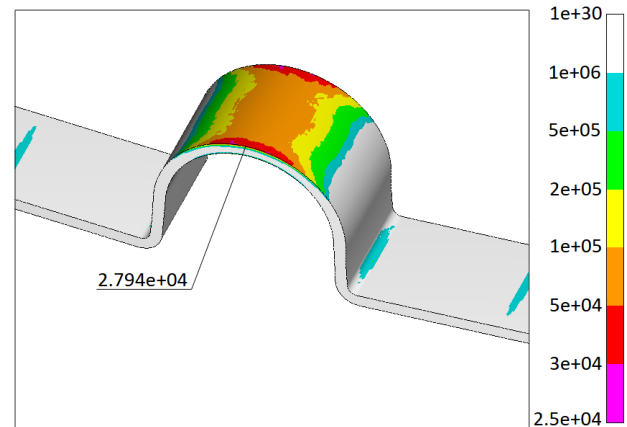


Figure 7. Calculated number of cycles until crack initiation based on MLSS, specimen A

3.2 Specimen B

Specimen B had an effective plastic strain at the critical spot of about 23% which is more than the uniform elongation. The material and thickness are the same as specimen A. Specimens were exposed to a three point bending test, where the loading cycle asymmetry was $R=0.067$. Dimensions of specimen B are shown in Figure 8a, the position of the critical spot is shown in Figure 8b.

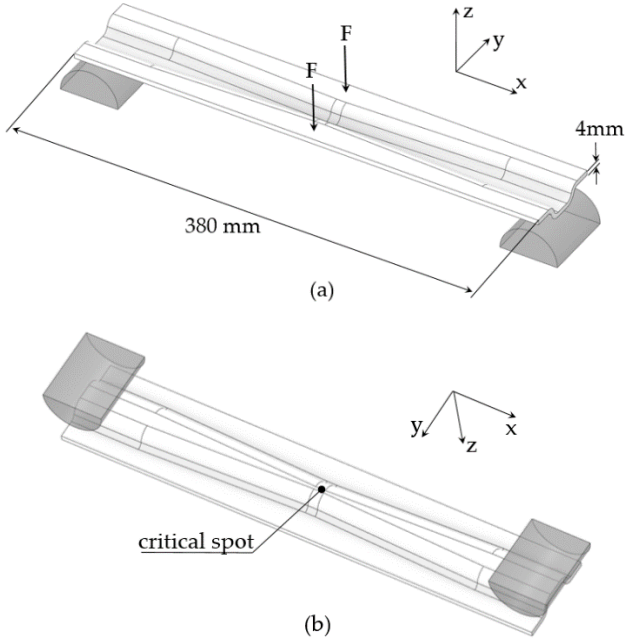


Figure 8. (a) Dimensions of specimen B, (b) position of critical spot

Three different loading levels were tested as shown in Figure 9. Good agreement between MLSS and the experiments can be seen. Some discrepancy may be caused by neglecting residual stress.

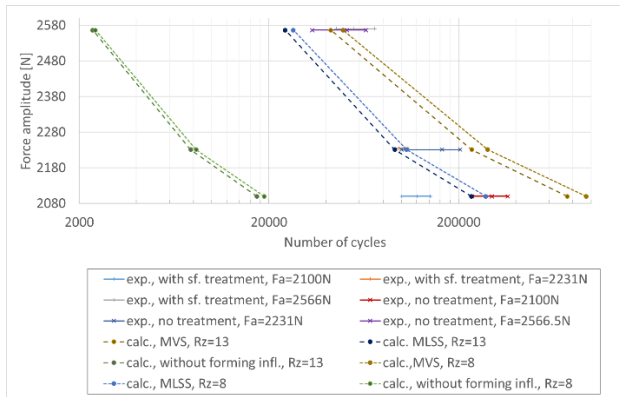


Figure 9. Specimen B - Experiments (exp.) and calculations (calc.) comparison

Stress amplitude and mean stress in the critical spot of specimen B is shown in Table 2.

Force amplitude [N]	Stress amplitude [MPa]	Mean stress [MPa]
2566.5	456	96
2231	400	97
2100	368	99

Table 2. Mean stress and stress amplitude in critical spot of specimen B

Specimen B with fatigue fracturing is shown in Figure 10. This specific specimen was tested with a force amplitude of 2100 N. The specimen was not treated with a surface coating.



Figure 10. Specimen B after testing

Figure 11 shows the calculated number of cycles until crack initiation. Force amplitude was 2100 N, surface roughness was $R_z=8 \mu\text{m}$ and MLSS was used in this case.

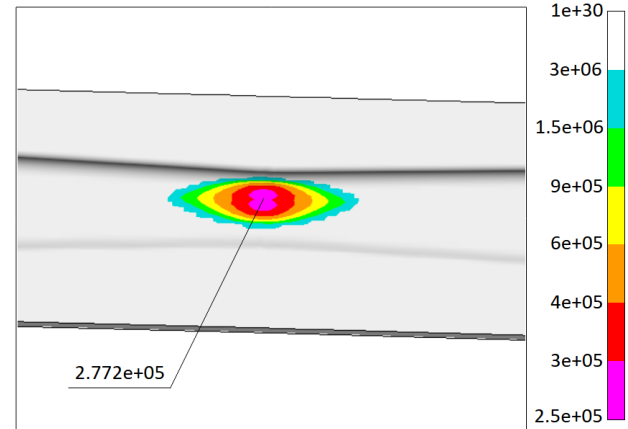


Figure 11. Calculated number of cycles until crack initiation based on MLSS, specimen B

3.3 Specimen C

Specimen C is a stabilizer clamp subjected to a three point bending test. Specimens were subjected to five different levels of loading. Only specimens with Zn-Ni surface coating were tested. Effective plastic strain at the critical spot was 51%. Clamps were made from S420MC. The metal sheet thickness was 3.5 mm. The clamp and its support used for the three point bending test is shown in Figure 12. Cyclic load asymmetry was $R=0.2$.

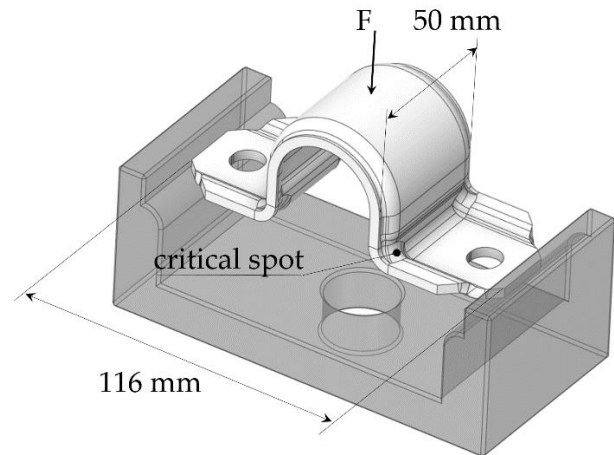


Figure 12. Three point bending test of specimen C

Figure 13 shows a comparison of the calculations and experiments. MLSS provided non-conservative results. Results provided by MVS were even more non-conservative.

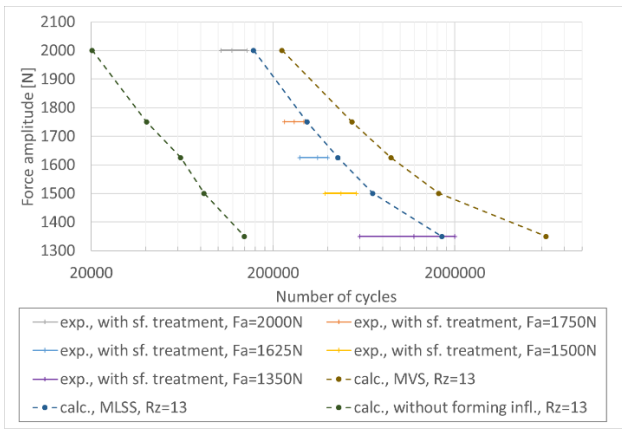


Figure 13. Specimen C – Comparison of experiments (exp.) and calculations (calc.)

Stress amplitude and mean stress in the critical spot of specimen C for each loading level are shown in Table 3. The values in the table are related to a model where the forming effect is not considered. If the forming effect is considered, then the position of the critical spot is moved slightly, which leads to slightly different stress values.

Force amplitude [N]	Stress amplitude [MPa]	Mean stress [MPa]
2000	601	-106
1750	525	-105
1625	480	-108
1500	451	-105
1350	407	-105

Table 3. Mean stress and stress amplitude in the critical spot of specimen C

Figure 14 shows specimen C after testing. The specimen in the figure was tested with a force amplitude of 1500 N.



Figure 14. Specimen C after testing

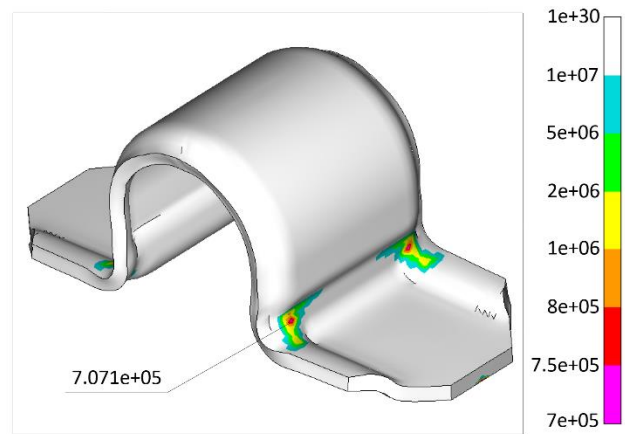


Figure 15. Calculated number of cycles until crack initiation based on MLSS, specimen C

Figure 15 shows the number of cycles until crack initiation. Force amplitude was 1500 N, surface roughness was $R_z=13 \mu\text{m}$ and MLSS was used in this case.

3.4 Specimen D

Specimen D is based on specimen A. One more forming operation was added which led to a change of the specimen shape and to the change of the position of the critical spot. Effective plastic strain at the critical spot was 48%. Material S420MC was used for the specimen. The specimens were exposed to symmetric compression-tension load cycles with three different force amplitudes, which differed from the amplitudes used for the A specimens. Specimens with Zn-Ni surface coating and specimens without surface treatment were tested. The dimensions of specimen D are shown in Figure 16. The left end of the specimen was not parallel with the right end of the specimen. This led to the creation of bending stress when the specimen was fixed into the testing machine. The effect of mean stress was considered as it was described earlier.

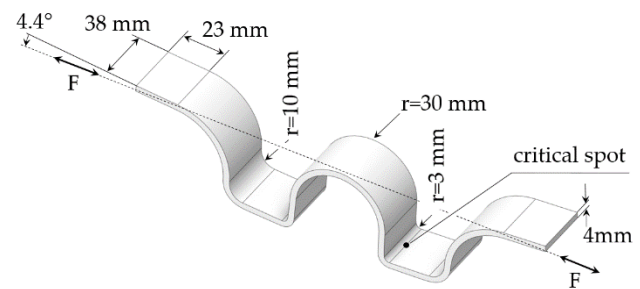


Figure 16. Dimensions of specimen D

Figure 17 shows a comparison between the calculations and experiments. The results based on MLSS and MVS are very different from the experimental results. The calculations where the effect of plastic strain was not considered are close to the experimental results.

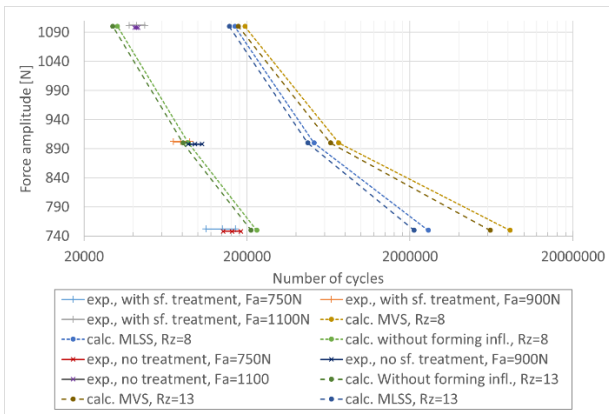


Figure 17. Specimen D – Comparison of experiments (exp.) and calculations (calc.)

Mean stress and stress amplitude in the critical spot of specimen D is shown in Table 4. The values in the table are related to a model where the forming effect is not considered. If the forming effect is considered, then the position of the critical spot is moved slightly which leads to slightly different stress values.

Force amplitude [N]	Stress amplitude [MPa]	Mean stress [MPa]
1100	497	67
900	410	76
750	344	90

Table 4. Mean stress and stress amplitude in critical spot of specimen D

Figure 18 shows specimen D after testing. The specimen in the picture was tested with a force amplitude of 1100 N and its surface was treated with Zn-Ni coating.

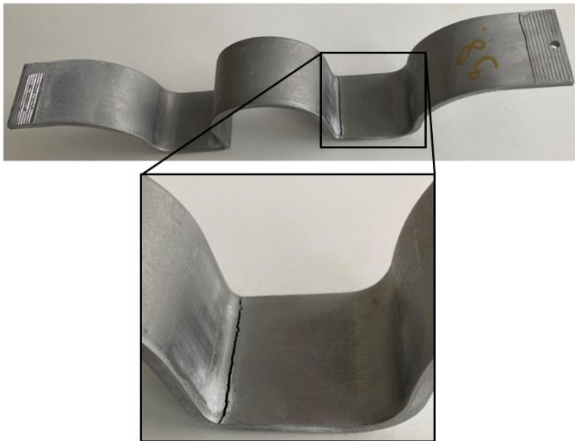


Figure 18. Specimen D after testing

Figure 19 shows the calculated number of cycles until crack initiation. Force amplitude was 1100 N, surface roughness was $R_z=13 \mu\text{m}$ and MLSS was used in this case.

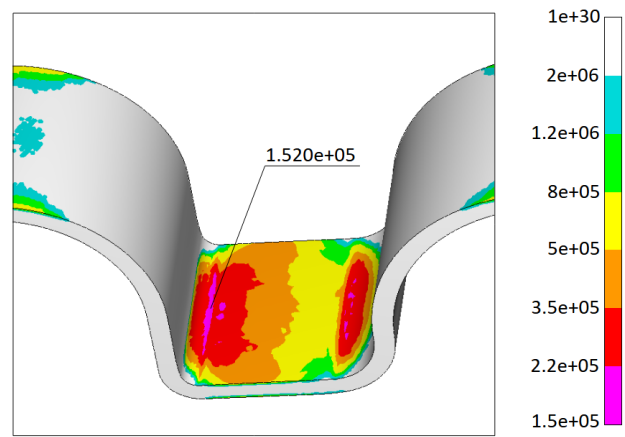


Figure 19. Calculated number of cycles until crack initiation based on MLSS, specimen D

The loading force was set up so that the rupture occurred in the high cyclic fatigue regime. The different shapes of the samples and the different strain φ_v in critical spots resulted in the different levels of stress amplitude, see tables 1-4.

4 PROCEDURE MODIFICATION

MLSS provided realistic results for specimens A and B where the effective plastic strain originating during forming was moderately low. When the method was used for specimen C, where effective plastic strain was high, then the results became non-conservative. MLSS highly overestimated the life-time of specimen D, where effective plastic strain is similar to specimen C. From our results, it follows that for areas with high effective strain the life-time prediction based on MLSS is not reliable.

Stamped parts usually contain areas of low strain where assumptions of MLSS are valid and areas of high strain where they are not. It is not convenient in engineering practice to distinguish these areas manually, because it could lead to mistakes. We present a simple approach for dealing with this.

One option is to modify the $S-N-\varphi_v$ surface (or $\varepsilon_\sigma-N-\varphi_v$ surface from Figure 2) and acquire something like that shown in Figure 20. As mentioned earlier, modification of proprietary fatigue software is not possible, so direct modification of the $S-N-\varphi_v$ surface cannot be done in it.

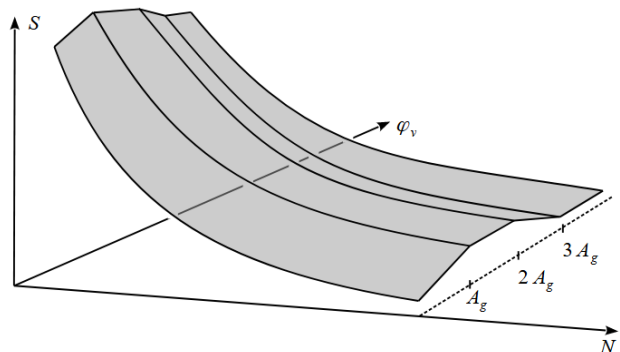


Figure 20. Modified dependence of S-N curve on effective plastic strain

Nevertheless, it is possible to manipulate the result file where the forming simulation results are stored. This manipulation has a similar effect to the direct modification of the $S-N-\varphi_v$ surface. Specifically FEMFAT 2022a, which we used, takes the forming results from an Abaqus .odb file, LS-DYNA result file or .erfh5 file. The .erfh5 file format was chosen because it can be easily manipulated in Python via library H5Py [Collette 2008]. Files of type .erfh5 are based on HDF5 technology [HDF Group 2006]. Libraries which enable the user to manipulate .erfh5 files in

other programming languages like C/C++, Fortran or Java are available at [HDF Group 2006]. Original effective plastic strain φ_v is changed to modified effective plastic strain $\hat{\varphi}_v$ during this process, see Figure 21.

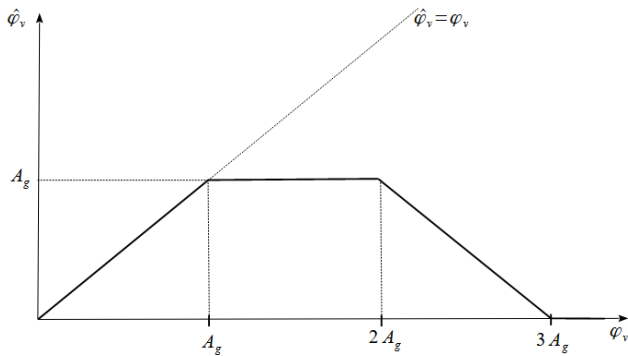


Figure 21. Conversion of effective plastic strain

The modified .erfh5 file where $\hat{\varphi}_v$ is stored is used for fatigue evaluation. The modified $\hat{\varphi}_v$ respects our observations based on the testing of specimens A-D. If effective plastic strain is lower than uniform elongation A_g then no modification is needed and the MLSS method is valid as it is. If effective plastic strain φ_v is between A_g and $2A_g$ then we recommend keeping $\hat{\varphi}_v$ constant. If effective plastic strain φ_v is higher than $2A_g$ then we recommend decreasing $\hat{\varphi}_v$ to zero. This is because the results from specimen D, which were calculated without the influence of effective plastic strain, fitted the experimental data the best.

Figure 22 compares the results from specimen A based on MLSS when the original (orig.) $S-N-\varphi_v$ is used and when the modified (modif.) $S-N-\hat{\varphi}_v$ is used. Effective plastic strain in the critical spot is lower than A_g , so there is no difference and the corresponding curves are identical. Figure 22 also shows the experimental results and the calculation results where the forming effect was not considered.

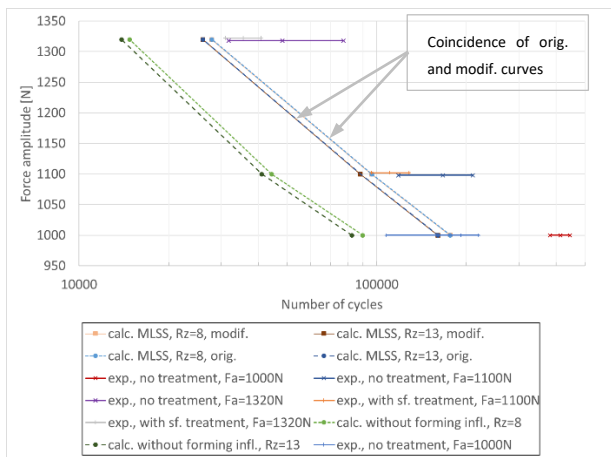


Figure 22. Comparison of results from specimen A

Figure 23 compares the results from specimen B. Results become slightly conservative if a modified $S-N-\hat{\varphi}_v$ surface is used. Nevertheless, these results are still closer to the experimental results than the results which neglect the forming effect completely.

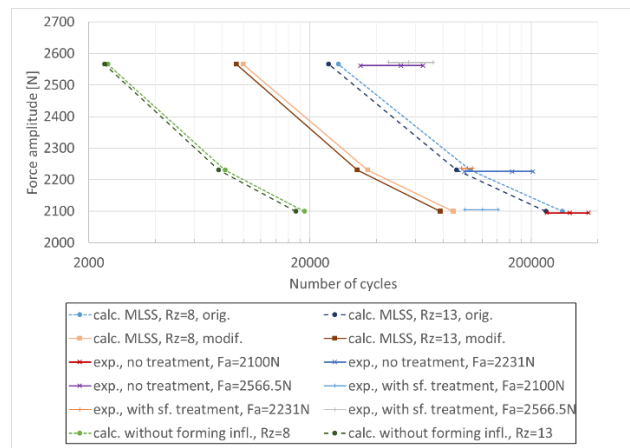


Figure 23. Comparison of results from specimen B

The highest risk of life-time overestimation was in the cases of specimens C and D. If a modified $S-N-\hat{\varphi}_v$ surface is used, then the risk is reduced. Figure 24 compares the results from specimen C. The modified $S-N-\hat{\varphi}_v$ surface made the results highly conservative. This is preferable to a situation when the life-time is overestimated. The curve corresponding to the MLSS and the modified $S-N-\hat{\varphi}_v$ surface became coincident with the curve representing the results without the forming influence.

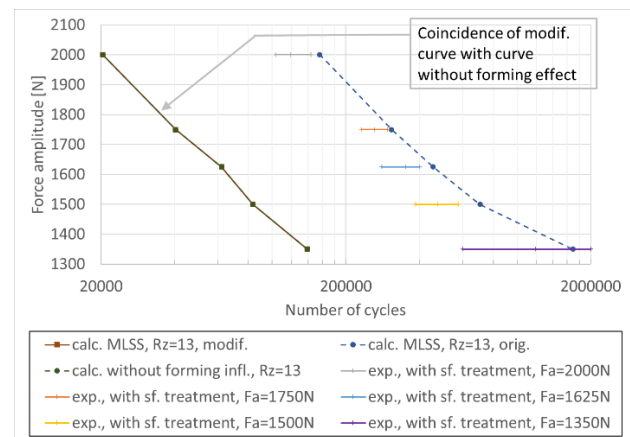


Figure 24. Comparison of results from specimen C

Figure 25 compares the results from specimen D. As can be seen, using the modified $S-N-\hat{\varphi}_v$ surface meant the MLSS results drew closer to the experimental ones. However, these results remained slightly non-conservative.

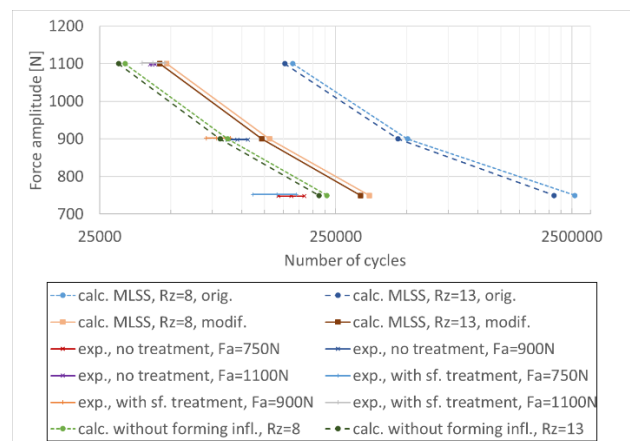


Figure 25. Comparison of results from specimen D

5 CONCLUSION

Fatigue testing of stamped parts with four different levels of pre-strain was performed over a high cyclic fatigue range. The results from the experiments and the calculations were compared. If the level of pre-strain was moderately low, then MLSS provided realistic results. Some discrepancies between experimental and calculated results were observed for high levels of pre-strain. Therefore, a simple correction method which prevents overestimation of fatigue life was proposed. The MLSS method and the modified $S-N-\hat{\phi}_v$ surface are helpful especially in the early design stages when rough life-time predictions are made.

It is not possible to derive a precise material law from only four different pre-strain levels. If our method is adopted by other researchers, then we recommend performing the effective plastic strain conversion based on their own data and observations.

This study showed that fatigue of bodies with high pre-strain levels is not well described. Further research should be focused on this area.

ACKNOWLEDGMENTS

This paper is based on the work sponsored under the project "Comprehensive support for designing technical equipment" SGS-2022-009 and in cooperation with MUBE A, spol. s.r.o. using their equipment and materials for specimen preparation.

REFERENCES

- [Abspoel 2013] Abspoel, M. et al. A new method for predicting Forming Limit Curves from mechanical properties. *Journal of Materials Processing Technology*, May 2013, Vol. 213, No. 5, pp 759-769, ISSN 1873-4774
- [Chval 2020] Chval, Z. et al. Topology optimization of B-pillar with respect to mesh type and size. *IOP Conference Series: Materials Science and Engineering*, Vol. 776, No. 1. DOI:10.1088/1757-899x/776/1/012025
- [Chval 2016] Chval, Z. et al. Design of mechanical forging press with maximal force in side cavity. *MM Science Journal*, November 2016, pp 1358–1361. DOI:10.17973/mmsj.2016_11_2016121
- [Collette 2008] Collette, A. HDF5 for Python. 2008. Available from <http://www.h5py.org>.
- [FEMFAT 2022] FEMFAT 2022a User Manual. 2022.
- [FKM 2003] FKM (Forschungskuratorium Maschinenbau), Analytical Strength Assessment of Components, 5th expanded edition (in German). VDMA Verlag, 2003. ISBN 3-8163-0479-6
- [Hatscher 2004] Hatscher, A. Estimation of the cyclic characteristics of steels (in German). Claushal: Papierflieger, 2004. ISBN 3-89720-719-2
- [HDF Group 2006] HDF Group. The HDF Group - ensuring long-term access and usability of HDF data and supporting users of HDF technologies. 2006. Available from <http://www.hdfgroup.org>.
- [Hill 1948] Hill, R. A theory of the yielding and plastic flow of anisotropic metals. *Proceedings of the Royal Society of London, Series A*, Vol. 193, 1948. DOI: <https://doi.org/10.1098/rspa.1948.0045>
- [Jakubec 2022] Jakubec, M. Anisotropy influence on sheet metal part fatigue life. Prague: Czech technical university in Prague, Faculty of mechanical engineering, 2022.
- [Klemenc 2015] Klemenc, J. Influence of fatigue–life data modelling on the estimated reliability of a structure subjected to a constant-amplitude loading. *Reliability Engineering and System Safety*, October 2015, Vol.142, pp 238-247, ISSN 1879-0836
- [Le 2009] Le, Q. et al. Modified strain-life equation to consider the effect of different prestrain paths for dual phase sheet steel. *Journal of Materials Processing Technology*, April 2009, Vol. 209, No. 7, pp 3525-2531, ISSN 1873-4774
- [Martinez 2019] Jimenez-Martinez, M. and Alfaro-Ponco, M. Fatigue damage effect approach by artificial neural network. *International Journal of Fatigue*, July 2019, Vol. 124, pp 42-47, ISSN 1879-3452
- [Massendorf 2000] Massendorf, R. The influence of forming on the cyclic material characteristic values of fine sheets (in German). Claushal: Papierflieger, 2000. ISBN 3-89720-413-4
- [Meng 2013] Meng, J. et al. Integration of multi-step stamping effect in the bending fatigue analysis of a steel wheel. *Fatigue & fracture of engineering materials & structures*, August 2013, Vol. 36, No. 8, pp 795-808
- [Raz 2020] Raz, K. et al. Unconventional design of the mechanical crank press developed by the topology optimization. *Manufacturing Technology*, Vol. 20, No. 3, pp 368–372. <https://doi.org/10.21062/mft.2020.047>
- [Wächter 2022] Wächter, M. et al. On scaled normal stresses in multiaxial fatigue and their exemplary application to ductile cast Iron. *Applied mechanics*, March 2022, Vol. 3, No. 1, pp 259-295. DOI: <https://doi.org/10.3390/applmech3010018>

CONTACTS:

Ing. Jaromir Kaspar
University of West Bohemia, Faculty of Mechanical Engineering, Department of Machine Design
Univerzitni 22, 306 14 Pilsen, Czech Republic,
tel. +420 778 203 443, e-mail: jkaspar@fst.zcu.cz

Ing. Petr Bernardin, Ph.D.
University of West Bohemia, Faculty of Mechanical Engineering, Department of Machine Design
Univerzitni 22, 306 14 Pilsen, Czech Republic,
tel.: +420 377 63 8263, e-mail: berny@fst.zcu.cz

prof. Ing. Vaclava Lasova, Ph.D.
University of West Bohemia, Faculty of Mechanical Engineering, Department of Machine Design
Univerzitni 22, 306 14 Pilsen, Czech Republic,
tel.: +420 377 63 8264, e-mail: lasova@fst.zcu.cz